Supplementary Information, (10 pages) for:

Morphologically and compositionally tuned lithium silicate nanorods as high-performance carbon dioxide sorbents.

P. V. Subha[a], Balagopal N. Nair[*b,c], A. Peer Mohamed[a], G. M. Anilkumar[b], K. G. K. Warrier[a], T. Yamaguchi[d] and U. S. Hareesh[*a,e]

[a]Materials Science and Technology Division (MSTD), National Institute for Interdisciplinary Science and Technology, Council of Scientific and Industrial Research (CSIR-NIIST), Pappanamcode, Thiruvananthapuram, Kerala 695019, India. [*]E-mail: hareesh@niist.res.in

[b]R&D Centre, Noritake Company LTD, 300 Higashiyama, Miyoshi, Aichi 470-0293, Japan. [*] E-mail: bnair@n.noritake.co.jp

[c]Nanochemistry Research Institute, Department of Chemistry, Curtin University, GPO Box U1987, Perth, Western Australia 6845, Australia

[d]Chemical Resources Laboratory, Tokyo Institute of Technology, Nagatsuta 4259, Midori-ku, Yokohama 226-8503, Japan

[e]Academy of Scientific and Innovative Research, Delhi−Mathura Road, New Delhi 110 025, India

Table of Contents

Section S1. Table S1 comparing the absorption performance of Li_4SiO_4 based absorbents from published literature

Material	Precursor	Synthesis method	Temperature (K)	Morphology	Absorption capacity (wt. %)	Time for absorption (min)	Rate of absorption (wt. % sec^{-1})*	Ref.
Li_4SiO_4	LiOH and Fumed silica.	solid-state	823	macro porous	28.1	5	0.093	(1)
Li_4SiO_4	Li and Si containing MOF	Solvothermal	773	Coral	29.4	5	0.04	(2)
			873	Coral	32.4	5	0.011	
Li_4SiO_4	$LiOH/C_6H_8O_7/SiO_2$	Citrate sol-gel	953	porous grains	30.1	20	0.025	(3)
Li_4SiO_4 based sorbent from diatomite	$LiNO_3$, Diatomite, $NH_3 \cdot H_2O$	Impregnation Precipitation	893	spherical	34.02	20	0.2125	(4)
Li_4SiO_4 $Li_{4x}Na_xSiO_4$	TEOS, Li_2CO_3, Na_2CO_3,	Coprecipitation	Dynamic run	Large and dense particles	Li_4SiO_4 = 12	(0-10)	Li_4SiO_4= 0.00159	(5)
					$Li_{3.85}Na_{0.15}SiO_4$ =19.3	(0-10)	$Li_{3.85}Na_{0.15}SiO_4$= 0.00743	
Li_4SiO_4, Li_2SiO_3, Li_2TiO_3	-	-	923	spheres	28.4	2	0.23	(6)
$Li_{3.9}Na_{0.1}Si_{0.96}Ti_{0.04}O_4$	$LiNO_3$, $Ti(OC_4H_9)_4$, $Si(OC_2H_5)_4$, NaOH, CH_3CH_2OH, $C_6H_8O_7$	Sol–gel	923	porous	32.6	60	0.009	(7)
Li_4SiO_4	Diatomiteas silicon source, Li_2CO_3	Solid state	973	porous	34.14	30	0.0189	(8)

*** Rate of absorption values calculated from absorption capacity close to maximum and time taken to reach that value as reported in the referred manuscripts.**

Section S2. Phase identification of the microwave sol-gel particles during its synthesis and TEM/HT-XRD plots of samples at various stages of heat treatment.

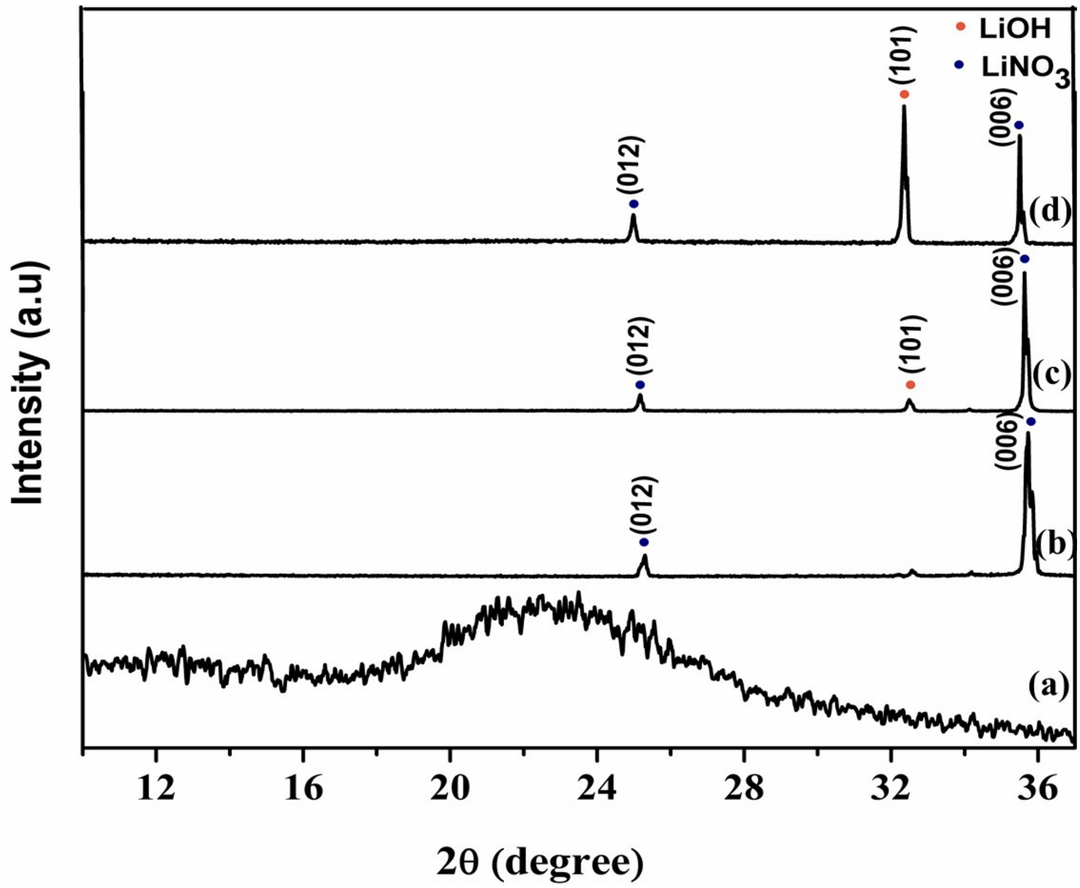

Fig. S1 Phase identification of precursors (a) Colloidal silica (b) $LiNO_3$ (c) the particles after sol gel process (d) the particles after microwave treatment (before any heat-treatment). ($LiNO_3$• JCPDS –01-080- 0203, LiOH•-01-085-0736).

Phase identification of the precursors used in the synthesis and their phase transformation during the synthesis is shown in Fig. S1. From the XRD plots, it is clear that colloidal silica exhibited amorphous nature and $LiNO_3$ showed its typical crystalline structure. After hydrolysis, LiOH peaks start appearing [Fig. S1(c)] while lithium nitrate still exists in the solution. The progress of hydrolysis of the lithium nitrate precursor on microwave treatment is clearly confirmed from the phase analysis by the relative enhancement in the (101) peak of LiOH [Fig. S1 (d)].

The phase change of the powder samples during heat treatment was traced using insitu HT-XRD (Rigaku RINT -TTR III) and the results are shown in Fig. S2. The morphology of the resulting powder samples have been analysed using TEM (HRTEM, FEI Tecnai 30 G2 S-

TWIN) and the results are included as Fig. S3. The spherical silica particles are clearly visible in the TEM images of the samples recorded after heat treatment to 473K as in Fig. S3. On further heat treatment the melting of unreacted lithium nitrate *(video file attached separately as Movie S1)* occurs at about 528K. TEM images of particles heat-treated after 673K, however, still show the presence of spherical silica particles (Fig. S3) and hence it can be concluded that the full digestion of the silica phase in the synthesis solution or the molten lithium nitrate salt never occurred at our processing conditions.

Samples analysed by HT-XRD showed that the reaction product was completely amorphous at 746K (Fig. S2). We believe that the good wettability of the molten lithium salt on the surface of silica limited the particle aggregation and promoted the arrangement of lithium coated silica particles along one dimension. The nucleation of Li_2SiO_3 should have occurred from this coated one dimensional array of amorphous silica particles between 746K and 773K leading to the formation of nanofibrous crystalline particles rich in lithium metasilicate phase (Fig. S2 and Fig. S3).

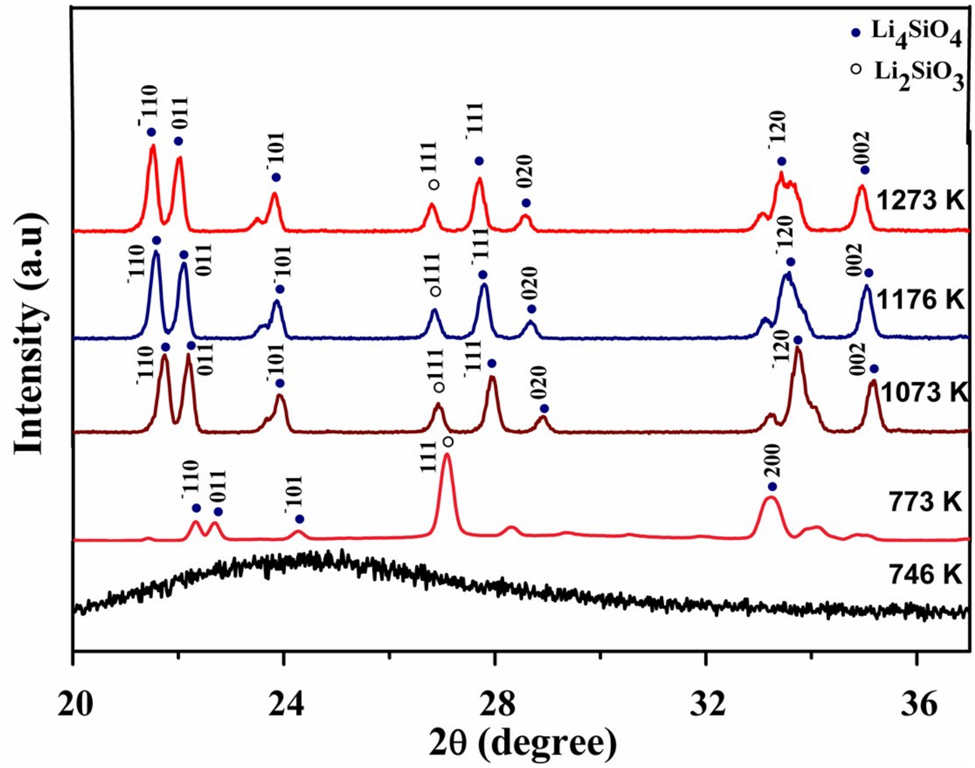

Figure S2. Phase characterisation of the microwave sol-gel synthesized particles during heat treatment analysed using in situ HT-XRD.

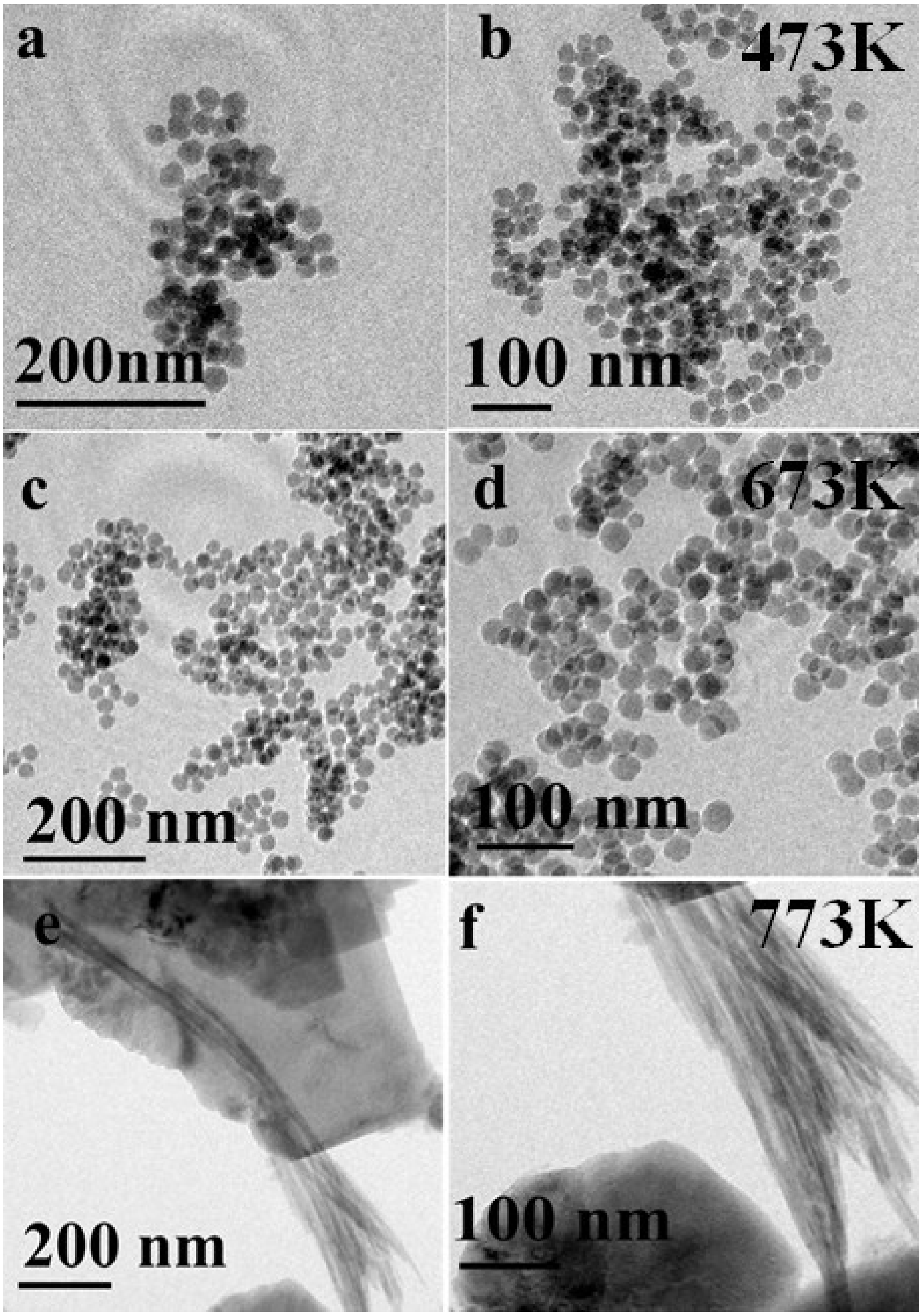

Fig. S3.TEM images of particles calcined at 473 K (a & b), at 673 K (b & c), 773 K (e & f).

On further heat-treatment to 1073 K, pure lithium orthosilicate phase formation occurred presumably at the expense of lithium meta silicate phase as revealed by the increase in the intensity of (-110) and (011) planes with the increase in temperature. The slight peak shift towards left observed in the XRD of the samples on heat-treatment may be due to the relaxation of the geometrically induced growth stress arising from the large volume expansion during lithium silicate phase formation

Section S3. N_2 adsorption based surface area measurement of lithium orthosilicate powder samples.

N_2 adsorption based surface area analysis was performed at 77K using Micromeritics Tristar 111 surface area analyser after degassing the sample at 200 °C for 2 h. Typical Type II adsorption isotherm was measured revealing the non-porous nature of the particles. The surface area of the particles was calculated as 7.3 m^2/g based on BET analysis.

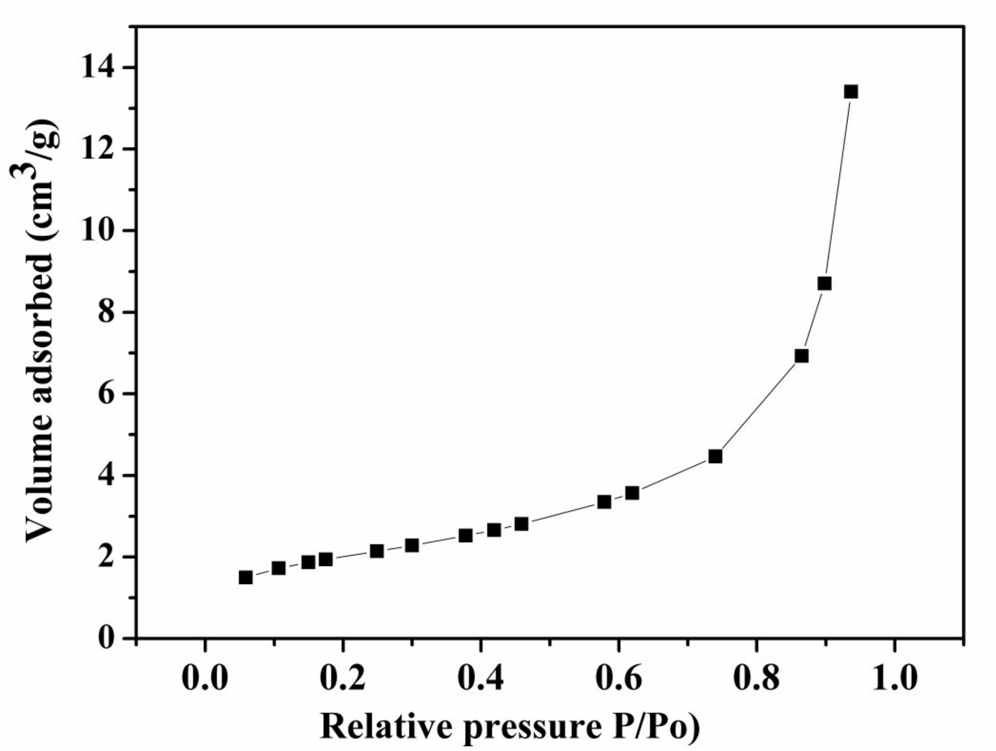

Fig. S4. N_2 adsorption isotherm of the particles synthesised through microwave sol-gel method (calcined at 1073K)

Section S4. X-ray diffraction patterns of samples before and after carbon dioxide absorption and after desorption.

The mechanism of CO_2 absorption and desorption in these materials is well known. The phase transition of the lithium silicate particlesonCO$_2$absorption and desorption are represented by the XRD curves in Fig. S5. The diffraction patterns of sample after CO_2 absorption [Fig. S5 (b)] indicated phases of lithium metasilicate and lithium carbonate. The XRD pattern of the samples after CO_2 desorption [Fig. S5 (c)] is similar to the sample before CO_2 absorption [Fig. S5 (a)] and all peaks could be indexed to Li_4SiO_4.

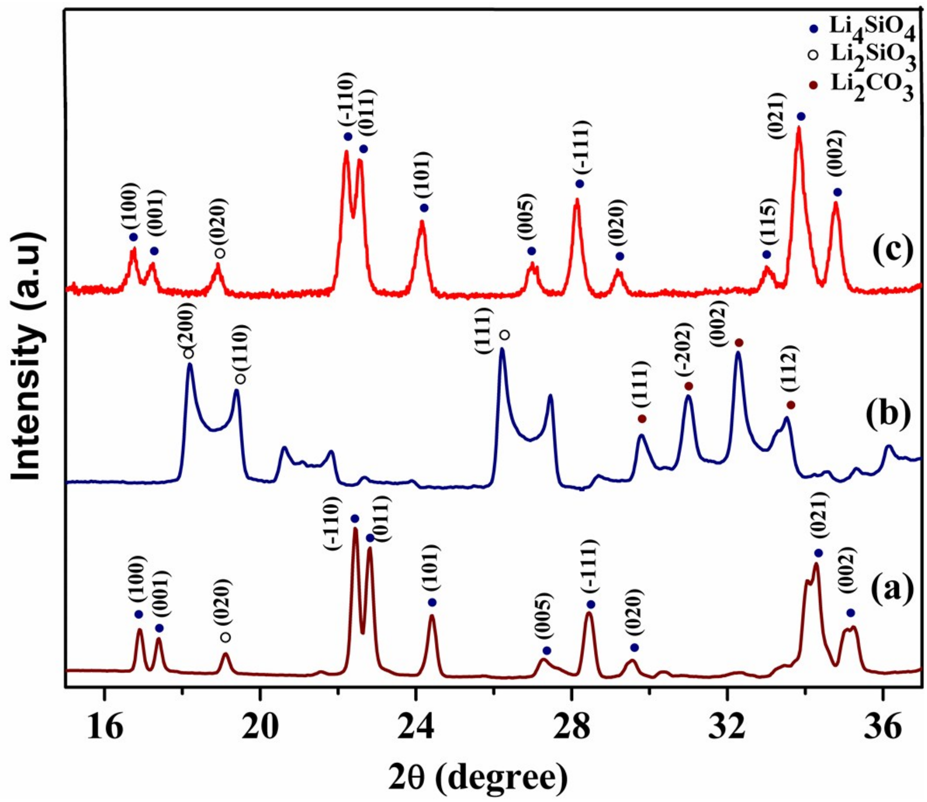

Fig. S5. X-ray diffraction patterns of (a) Li_4SiO_4 particles before CO_2 absorption (b) Particles after CO_2 absorption process (c) Particles after desorption process.

The morphology and crystallinity of the powders on CO_2 absorption/desorption were further characterised using TEM analysis (HRTEM, FEI Tecnai 30 G2 S-TWIN operated at an accelerating voltage of 300 kV) and its detailed results are reported in the manuscript. The corresponding SAED patterns are shown in Fig. S6 here. The results in Fig. S6 confirm the full reversibility of the Li_4SiO_4 crystalline strucutre on adsorption/desorption cycle.

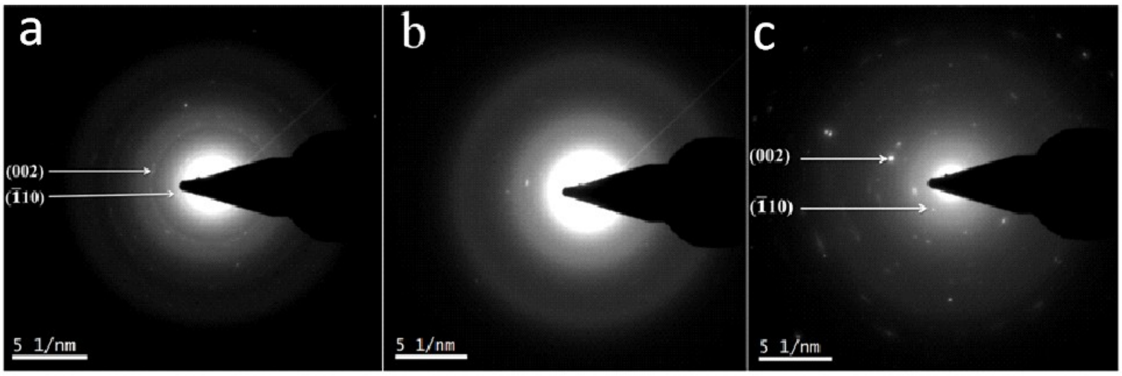

Figure S6. Selected area electron diffraction (SAED) patterns of (a) Li_4SiO_4 particles before CO_2 absorption (b) Particles after CO_2 absorption process (c) Particles after desorption process

Section S5. Kinetic studies on microwave sol-gel sample and Eutectic-3 composition

To understand more about the CO_2sorption process, the absorption curves as in Fig. 2e of the manuscript were fitted using a double exponential model

$$Y = A.Exp^{-K_1 x} + B.Exp^{-K_2 x} + C$$

Where, Y represents the amount of CO_2 absorbed at the time "x". K_1 and K_2 are the exponential constants for the absorption of CO_2 on the surface of the particles and the part of absorption kinetically controlled by the bulk diffusion processes respectively. The K_1 and K_2 values calculated for the samples are displayed in Table S2 below. Regression values close to 1 as shown in Table S2 revealed extremely good fittings for all curves. K_1 values are usually ~10 times larger than that of K_2 ; the trend is reversed in the present study as shown in Table S2. Larger K_2 values as in here represents, faster lithium ion diffusion to the reaction interface compared to the chemisorption reaction there.

Table S2. Kinetic parameters obtained from the absorption curves of Li_4SiO_4 at various temperatures when fitted to a double exponential model

Temperature (K)	K_1(1/s)	K_2(1/s)	R^2
723	0.00015	0.0013	0.999
773	0.00025	0.0034	0.999
873	0.00026	0.0064	0.998
923	0.00046	0.0189	0.993

The absorption curves at different temperatures of the Eutectic-3 composition (as in Fig. 5a) were also fitted to the double exponential model and the resulting kinetic parameters were used to fit the Arrhenius plot in Fig. 5c of the manuscript. The calculated kinetic parameters at various temperatures are tabulated in Table S3 below.

Table S3. Kinetic parameters obtained from the CO_2 absorption curves of Eutectic-3sample containing Li_4SiO_4 at various temperatures

Temperature (K)	K_1(1/s)	K_2(1/s)	R^2
673	0.000024	0.000024	0.998
723	0.00069	0.00069	0.996
823	0.036	0.0282	0.997
873	0.1655	0.081	0.981

References

[1] H. Kim, H. D. Jang, M. Choi, *Chem. Eng. J.* **2015***,* **280**, 132.

[2] J. H. Lee, B. Moon, T. K. Kim, S. Jeoung, H. R. Moon, *Dalton Trans*. 2015, **44**, 15130.

[3] K. Wang, X. Y. Wang, P. F. Zhao, X. Guo, *Chem. Eng. Technol.* **2014,** 37, 1552.

[4] S. Shan, S. Li, Q. Jia, L. Jiang, Y. Wang, and J. Peng. *Ind. Eng. Chem. Res*. **2013,** 52, 6941.

[5] V. L. Mejı´a-Trejo, E. Fregoso-Israel, *Chem. Mater.* **2008,** 20, 7171.

[6] R. Quinn, R. J. Kitzhoffer, J. R. Hufton, T. C. Golden, *Ind. Eng. Chem. Res.* **2012,** 51, 9320.

[7] M. Xiang, Y. Zhang, M. Hong, S. Lou, Y. Zhang, H. Liu, C. Gu, J. Mater. Sci. **2015,** 50, 4698-4706.

[8] S. Shan, Q. Jia, L. Jiang, Q. Li, Y. Wang, J. Peng, *Ceram. Int*. **2013,** 39, 5437.